Journal of Colloid and Interface Science 409 (2013) 245–254

Contents lists available at ScienceDirect

Journal of Colloid and Interface Science

www.elsevier.com/locate/jcis

Preparation of multicompartment sub-micron particles using a triple-needle electrohydrodynamic device

Sheyda Labbaf [a,*], Sanjukta Deb [d], Giuseppe Cama [d], Eleanor Stride [b,c], Mohan Edirisinghe [a,b]

[a] Department of Mechanical Engineering, Biomaterials Research Laboratory, University College London, Torrington Place, London WC1 7JE, UK
[b] Department of Mechanical Engineering, University College London, Torrington Place, London WC1 7JE, UK
[c] Institute of Biomedical Engineering, Oxford University, Oxford OX3 7DQ, UK
[d] King's College London, Guy's Hospital, London SE1 9RT, UK

ARTICLE INFO

Article history:
Received 27 June 2013
Accepted 12 July 2013
Available online 30 July 2013

Keywords:
Electrohydrodynamic
Multilayered structures
Polymer
Drug delivery
Sub-micron particles
Human osteoblast cells

ABSTRACT

Control over the size and morphology of polymeric carriers for drug delivery systems is essential to optimize their functionality. In the current study, we demonstrate the feasibility of using an electrohydrodynamic process with a triple-needle device to prepare nearly mono-dispersed, spherical, tri-layered sub-micron particles. Three biocompatible polymer solutions of poly (lactic-*co*-glycolic acid) (PLGA), polycaprolactone (PCL) and polymethylsilsesquioxane (PMSQ) were used to prepare particles with three distinct layers. Optimized particles were shown to be spherical with an average size ranging from 320 nm (±80 nm) to 220 (±8 nm), which varied with a change in the working distance in the electrohydrodynamic processing. The surface and internal structure and morphology were studied using confocal, transmission and scanning electron microscopy combined with focused ion beam sectioning. Cytotoxicity was shown to be negligible in an *in vitro* assay. The ability to fabricate such multilayered particles in a single step, under ambient conditions has considerable potential for a range of applications in particular controlled release drug delivery system.

1. Introduction

Despite global interest, the development of single step processes for the preparation of effective drug delivery systems still faces numerous challenges. There is great demand for processing methods that are efficient, flexible, scalable and economical for the generation of a wide range of encapsulated nanostructures. A number of processes that have been established for the generation of multicompartment particles for medical applications include self-assembly [1], emulsion polymerization [2], layer-by-layer adsorption onto solid core particles [3], templated polymerization [4,5] and electrohydrodynamic atomization [6]. All these methods have their strengths and weaknesses, and technologies with the potential to create custom-tailored multicompartment particles are on the horizon. Nevertheless, over the past few decades, electrohydrodynamic (EHD) processing has received significant attention as a new method for the preparation of complex structures with attractive features for therapeutic applications. This technique avoids many of the processing problems that may interfere with drug encapsulation encountered with other techniques such as high temperature, agglomeration, protein denaturation and also the use of surfactant and/or organic solvents that may remain in the structures following processing leading to undesirable reactions with cells [7,8].

EHD processing enables the production of nanoscale particles with a controlled size distribution. Encapsulation studies using coaxial EHD processing, whereby two or more concentric liquid jets are formed simultaneously, present great potential for delivery systems i.e. carrier vehicles and multilayered capsules [9]. The ultimate aim of a drug delivery system is to have a regulated release profile from the desired drug carriers. Hence, preparation of multicompartment structures will enable more controlled release of drug over longer period of time. For this purpose, often biodegradable and biocompatible polymers are used in delivery vehicles to encapsulate or entrap therapeutic agents. Such materials are widely used as they allow sustained and controlled release of the encapsulated drug through diffusion and degradation in vivo [10,11]. Delivery vehicles loaded with an entrapped therapeutic agent can transport the substance through blood vessels to release their payload at a target site [12]. The co-delivery of synergistic drug combinations, with spatial and temporal control is important in targeted drug delivery. The current study focuses on the use of three different biocompatible polymers; poly (lactic-*co*-glycolic acid) (PLGA), polycaprolactone (PCL) and polymethylsilsesquioxane (PMSQ) to prepare tri-layered sub-micron particles. Recently,

* Corresponding author.
E-mail address: s.labbaf@ucl.ac.uk (S. Labbaf).

0021-9797/$ - see front matter © 2013 Elsevier Inc. All rights reserved.
http://dx.doi.org/10.1016/j.jcis.2013.07.033

PLGA and PCL have both been shown to be attractive candidates for biomedical applications due to their ability to degrade into natural metabolites and their non-cytotoxic nature [13]. PMSQ has also received considerable attention for the preparation of drug carriers as it is also non-toxic and has superior chemical and physical stability during drug release [14,15].

During EHD processing, the simultaneous flow of liquids in co-axially arranged needles under electrical potential differences is used to generate stable structures with a controlled size distribution [16]. By incorporation of an extra co-axial needle it is possible in principle to produce further layers. Although EHD processing is considered relatively easy to perform, attaining a specific size, size distribution, monodispersity and morphology of a desired type of particle is still challenging. Various parameters such as the magnitude of the electrical potential difference, flow rate, the collection plane and the physical properties of processed solution play an important role in creating an optimized structure [8,17,18]. The current study utilizes the EHD method combined with a triple-needle device for the preparation of multilayered structures using different polymeric materials. The study describes the use of the device to prepare unique structures, through a single step process, that holds great potential for the development of future drug delivery systems.

The co-axial method enables direct encapsulation of different drugs inside polymeric carriers, with desired size, in a single step. To the best of our knowledge, to date, only Ahmad et al. [18] have applied the EHD method combined with a coaxial triple-needle device to prepare a variety of multilayered structures using materials such as olive oil and glycerol. However, based on the data presented, the fabricated particles were agglomerated [18]. This led to difficulties in distinguishing individual layers. Therefore, the main aim of the current study was to investigate the feasibility of using triple-needle device, in combination with changes in the working distance, to design and produce an optimized electrospraying process that would allow the production of discrete, spherical, tri-layer sub-micron particles with a narrow size distribution via a single stepprocess using biomaterials. Importantly, the cytotoxicity of tri-layered sub-micron particles was assessed in order to confirm the absence of any toxic residue that may have remained following electrospraying. These are crucial aspects of the technology that need to be studied and understood prior to progressing to drug loading.

2. Experimental section

2.1. Materials

Three different polymers were used in this study; polymethylsilsesquioxane (PMSQ) powder provided by Wacker Chemie AG, GmbH, Burghausen, Germany. Poly (lactic-*co*-glycolic acid) (PLGA-co-polymer 50:50 Resomer RG503H, molecular weight 33,000 g/mol) was purchased from Boehringer Ingelheim, Germany. Calcein blue, Methyl green, Evans blue, polycaprolactone (PCL) (Mn 45,000) and solvents including ethanol (EtOH), dimethyl carbonate (DMC), dichloromethane (DCM) were all purchased from Sigma–Aldrich Poole, UK.

2.2. Solution preparation

PLGA, PCL and PMSQ solutions were prepared by mixing appropriate amounts of polymer with the relevant solvents (Table 1) and stirring for 900 s at the ambient temperature (21 °C), pressure and humidity.

Table 1
Physical properties of the solutions and solvents used in the study.

Sample	Viscocity (mPa s)	Surface tension ($mN\ m^{-1}$)	Electrical conductivity $\times 10^{-4}$ ($S\ m^{-1}$)
DMC:PLGA 95:5	3.1	27.7	0.2
DCM:PCL 94:6	6.3	24.7	0.1
EtOH:PMSQ 88:12	1.6	22.5	9

2.3. Characterization of polymer solutions

For the proposed study, viscosity, surface tension and electrical conductivity were measured as follows: Viscosity was measured using a VISCOEASY rotational viscometer (Brookfield Rheometer). Surface tension was measured using a Kruss Tensiometer (Standard Wilhelmy's plate method). Electrical conductivity was estimated using a HI-8733 (Hanna Instrument, USA) conductivity probe. The polymer solution properties are listed in Table 1. In all cases the mean value of five consecutive readings was taken.

2.4. Electrohydrodynamic (EHD) processing

In EHD processing an electric field is applied to a liquid droplet and the body of the liquid becomes charged; electrostatic repulsion offsets the surface tension and a droplet forms at the end of the needle (Fig. 1a). At a specific applied voltage (generated in this study by a high voltage power supply, Glassman Europe Ltd., Tadley, UK) and flow rate (controlled using high precision syringe pumps, Harvard Apparatus, Edenbridge, UK), the droplet adopts a conical shape and a fine jet emerges from its apex. The jet subsequently breaks up to form droplets. This is known as the stable 'cone-jet' mode [19] and is typically required in order to achieve fine particle production [20]. In this study, three coaxial liquid streams were produced simultaneously to form multilayereddroplets. It is believed that minimum droplet size can be achieved by increasing the applied voltage to the highest possible value and reducing flow rate to the lowest possible value whilst obtaining a stable cone-jet [21]. Moreover, according to Hartman et al [22], the shape of the cone-jet is as a result of an equilibrium between several forces of liquid pressure, liquid surface tension and the electrical stresses in the liquid surface. To form a stable 'cone-jet' the surface tension has to be overcome by the electric stress.

The dimensions of the needles used are shown in Fig. 1b. PLGA solution was introduced through the outer needle whilst the central and inner needles were supplied with PCL and PMSQ solutions, respectively. 10 ml volume capacity syringes were connected to each needle accordingly and were set at a specific flow rates (Table 2). Details of the applied voltage and the distance from the exit of the outer needle to the collector (known as working distance) for the current study are also shown in Table 2. All samples were collected in a petri dish filled with ethanol. Following droplet formation, the solvent evaporates leading to particle formation in the collecting media. All studies were carried out at the ambient temperature (21 °C), pressure and humidity.

2.5. Characterization techniques

Dynamic light scattering (DLS, Malvern instrument 2000) was applied to investigate the size distribution of multilayered nanospheres in 100% EtOH.

In order to confirm the presence of three different polymers in the produced particles, Fourier Transform Infrared (FTIR) spectra and Nuclear Magnetic Resonance (NMR) were both applied. FTIR

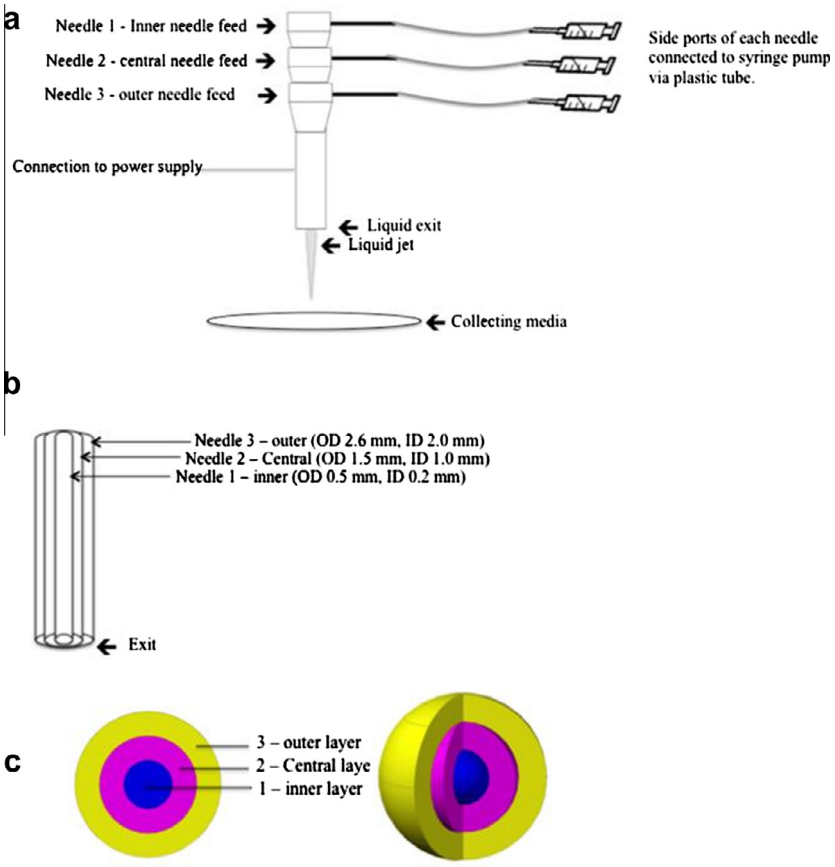

Fig. 1. Schematic illustration of (a) the experimental set-up for EHD processing using a triple-needle device for the fabrication of tri-layer particles and (b) the coaxial needle arrangement with labeled dimensions. ID and OD indicate internal and outer diameters, respectively. (c) Synthetic scheme illustration of a tri-layered structure both in 2D and corresponding 3D cross-section.

Table 2
Summary of the conditions used for the preparation of each sample. In all cases, 5 wt% PLGA, 6 wt% PCL and 12 wt% PMSQ solutions were used.

Sample	Sample ID	Voltage (kV)	Flow rate (μl/min)	Working distance (mm)
PLGA–PCL–PMSQ	PPP1	6.9–7.9	300–50–5	50
PLGA–PCL–PMSQ	PPP2	6.9–7.9	300–50–5	100
PLGA–PCL–PMSQ	PPP3	6.9–7.9	300–50–5	150
PLGA–PCL–PMSQ	PPP4	6.9–7.9	300–50–5	200
PLGA–PCL–PMSQ	PPP5	6.9–7.9	300–50–5	300

was performed on a Perkin–Elmer Spectrum 2000 spectrophotometer in the range of 350–4000 cm^{-1}.

^{13}C NMR spectra were measured on a Bruker AVANCE III 600 spectrometer equipped with a dual channel $^{1}H/^{13}C$ cryoprobe with the sensitivity optimized for ^{13}C measurements (150.9 MHz).

Confocal microscopy was applied to analyze the presence of a tri-layered structure. Each layer was labeled with the chosen dye. Calcein blue, methyl green and Evans blue were used to label PLGA (outer), PCL (middle) and PMSQ (inner) respectively. Briefly, 0.25 g/ml of dye was mixed with the polymer solution prior to being electrosprayed. The particles were collected on a glass cover slips for further analysis. Stained particles were viewed under an inverted confocal microscope (Zeiss LSM 710, Leica, Germany).

To study the structure, morphology and cross-section of the particles, Scanning Electron Miscroscopy (SEM) with Focused Ion Beam (FIB) milling (Carl Zeiss XB1540 "Cross-Beam") was used. The samples were collected on a glass cover slip and dried for 1 h prior to imaging. Following drying, samples were gold coated for 2 min via sputtering (Edward sputter coater) to improve the conductivity of the sample surface.

For Transmission Electron Microscopy (TEM) imaging, particles were dispersed in 100% EtOH and collected on a formvar/carbon on 400 mesh copper TEM grids and were then air-dried prior to analysis. TEM studies were performed on the JEOL-2000FX TEM, with an operating voltage of 80 kV and a 10 μm objective aperture to increase mass-thickness contrast. In order to check for the uniformity between different particles in one sample i.e. whether the outer and middle layer to radius of particles always remained a constant ratio, Image J software was used to measure the diameter and thickness of individual particles. The data were then plotted on a graph using Microsoft Excel for further analysis. The ratio of the layer thickness to overall radius of the sub-micron particles are presented by the gradient of linear regression line of the plotted graphs.

2.6. In vitro cell culture

It was important to assess the potential cytotoxicity of the formed particles. A primary human osteoblast (HOB) cell model was used for the current study as previously described by Di Silvio et al [23]. HOB cells were cultured in Dulbecco's modified Eagle's medium (DMEM), supplemented with 10% fetal calf serum (FCS),

1% non-essential amino acids, L-ascorbic acid (0.150 g/l), 1% of 200 mM L-glutamine, 2% of 1 M HEPES, penicillin (100 U/ml) and streptomycin (0.1 mg/ml) (All from Sigma, UK). HOBs were cultured at 37 °C in a 5% CO_2: 95% air atmosphere.

2.7. MTT Assay

Cell metabolic activity and consequently cell viability over time was assessed using the MTT [-(4,5-Dimethylthiazol-2-yl)-2,5-diphenyltetrazolium bromide] colorimetric assay. Test materials were soaked in 10 ml of DMEM media and placed onto a roller for 6 and 24 h to obtain the eluants. The cells were seeded at a density of 1×10^4 cells per well of a 96-well flat-bottomed plates and incubated for 24 h. Subsequently, 100 μL of eluant from the particles was added to the designated wells. The negative control contained media only whilst the positive control used was 10% alcohol diluted media. The cells were further incubated for 24 h in an incubator and MTT reagent was added to each well. After 4 h of incubation, dimethylsulfoxide (DMSO) was added to each well to dissolve formazan precipitates, and the absorbance was measured at 570 nm. Six replicate samples were analyzed for each eluant and the average amount of surviving cells for each sample were normalized with respect to the negative control. The data from the MTT assay were analyzed statistically by ANOVA and Kruskal–Wallis One Way Analysis of Variance on Ranks test at 5% significance level.

2.8. Live/dead staining

Live/dead assay (Invitrogen) was also used to assess cell viability/cytotoxicity. Live and dead assay is a commonly used two-color fluorescence-based method for determining viability of adherent or non-adherent cells. 1×10^5 cells per well of 24-well plates were left to grow in presence of the tri-layered particles for 24 h and subsequently stained with 4 μM Calcein AM and 2 μM Ethidium homodimer-1 in PBS for 30 min. The viability of the cells was observed under the fluorescent microscope (Olympus XI51).

2.9. Osteoblast cytoskeletal structure

HOBs were seeded at a density of 1×10^5 cell per well of 24-well plates. After incubation for 24 h in presence of the samples, cells were fixed for 5 min in 3.7% formaldehyde solution in phosphate buffer saline solution (PBS), then washed extensively and permeabilized with 0.1% TRITON X-100 in PBS. Afterwards, cells were stained with 50 mg/ml fluorescent phalloidin (Invitrogen, USA) conjugate solution in PBS for 40 min at ambient temperature and then washed several times to remove unbound phalloidin conjugate. A fluorescence microscope (Olympus XI51) was used to visualize the cytoskeleton organization.

3. Results and discussion

3.1. Preparation of multilayer structure

Fig. 1 illustrates the procedure for the preparation of particles via EHD processing (detailed procedure in materials and method section). The fabrication route was found to be successful for producing spherical and multilayered sub-micron particles of PLGA–PCL–PMSQ with a narrow size distribution. When immiscible liquids are injected, at specific flow rates, through electrified capillary needles, the menisci of all liquids (in this case three liquids) adopt a conical shape with an outer meniscus surrounding the inner ones. Solution properties play an important role in both obtaining a stable cone-jet mode and producing dispersed particles in an EHD process. EHD primarily requires the transfer of electric charge from the electrode to the droplet at the terminus of the tip. A minimum electrical conductivity in the solution is essential for electrospraying (Table 1). Nevertheless, it is often the surface tension and viscosity of the solutions that determine the window which a specific polymer/solvent combination can be EHD processed. According to Table 1, the surface tension values of the three solutions applied in this study were relatively similar. This enables the fabrication of a multilayer structure, as it allows the solutions to flow as one and therefore interact with one another.

It was found that viscosity of the polymer solution contributes significantly to the formation of multilayer particles. All three solutions displayed a range of viscosities (Table 1). It is important to couple materials with low viscosities with those that have higher values to enable formation of a more compact structure and also to achieve a more efficient encapsulation. In this study PCL solution, used in the central needle, was identified as the most viscous solution. To date, the data presented on the particles produced via EHD process have mainly focused on inviscid or moderately viscous liquids. This may be due to the fact that a stable cone-jet is difficult to achieve for a highly viscous liquid [24]. Based on the findings of Ku and Kim [24], for a highly conducting and viscous liquid, theelectrosprayed droplet sizes are comparatively insensitive to applied voltage and that the electrosprays assisted by corona discharge results in homogenous droplets if the corona intensity is not too high [24,25]. In EHD processing, the concentration should be sufficient enough to destabilize the charged jet that breaks down into small spherical droplets, which solidify during the course and are deposited on the collector. Nevertheless, it must be noted that too high a concentration cannot be chosen for particle production as it will interfere with solvent evaporation from one layer to another during processing. If the polymer concentration is too high then larger particles are obtained due to increased polymer mass in each droplet which would ultimately leave more solid in each particle following solvent evaporation. High polymer concentration would lead to premature drying of the droplet at the orifice tip while too low a concentration results in solvent saturation at the collector. In addition, chain entanglements play a crucial role in the physical properties of the particles produced. At low concentrations, there are fewer chain entanglement possibilities, where the operating regime is known as the semidulute unentangled regime [26]. In this case, the concentration is large enough to allow chain overlap but not enough to produce a significant degree of entanglement [26,27]. With increasing concentration, the same available hydrodynamic volume is engaged by more polymer chains, introducing chain entanglement [27]. The border of concentration from the semidilute unentangled to semi-dilute entangled regime was described by Gupta et al [27] as critical entanglement concentration,C_{ent}. There are some scaling laws to determine C_{ent} for each type of polymer, however it is more likely to be determined experimentally. Based on experimental data the concentrations of 5 wt% PLGA, 6 wt% PCL and 12 wt% PMSQ solutions were chosen for further study since they resulted in a stable 'cone jet' mode and subsequently the optimized multilayered particles (data from the optimization process are not shown).

3.2. Effect of working distance on particle size and size distribution

One of the main control parameters of the EHD process that is known to have an effect on the particle size is the working distance, classified as the distance between the droplet formation and collection. This phenomenon was investigated in this study (Table 2). It was found that increasing working distance, from 50 to 350 mm, led to the average particle size decreasing from 320 nm (±80 nm) to 220 nm (±8 nm) (Table 3 and Fig. 2). The graph presented in Fig. 2, generated by dynamic light scattering (DLS),

displays a shift to the left, confirming a reduction in the overall size of the particles with increased working distance. Also, it was demonstrated that with increased working distance the size distribution becomes narrower (Fig. 2) and hence polydispersivity becomes lower (Table 3).

The difference in the size and size distribution (Table 3 and Fig. 2) of the particles can be attributed to the solvent diffusion/evaporation. With increased working distance, the solvent evaporation increases due to longer time before reaching the collecting media. This would subsequently result in reduced solvent mixing with the collecting media following collection. As a result, the relative drying time (directly proportional to working distance) for the particles is significantly higher with increased working distance.

Another factor contributing to the reduction in size with increased working distance is the change in surface area of the droplets prior to collection in the solidifying media. With increasing surface area, the rate of solvent diffusion/evaporation, and subsequently particle solidification increases, leading to smaller particles. Ideally, the layers should not interfere with each other except that the liquid, from each layer, should diffuse out and the rate at which it diffuses would alternatively have an effect on the final particle size. During EHD processing, as the droplets break-up from the jet, the outer shell instantly becomes exposed to a non-solvent medium causing phase separation. The rate of phase separation is dependent upon how much non-solvent is effectively attacking the solvent of the outer shell at one time per unit volume. Therefore, it is suggested that if the particle size is smaller, this initial attack is more effective resulting in a polymerrich and polymer poor regions that may be associated with the kinetics and thermodynamics of polymer solutions [28]. Following this attack, polymer rich layer would diffuse into the inner side of the particle resulting in the liquid that attempts to escape, implying that the solidification process becomes faster and hence particle size smaller. Overall, with increased distance the droplet has a longer time to stabilize and form solidified sub-micron particles, from jet break-up time to entering the collecting media.

Table 3
The size distribution data for the multilayered PLGA–PCL–PMSQ structures.

Sample	Average size (nm)	Standard deviation (±nm)	Polydispersivity (%)
PPP1	320	80	25
PPP2	265	40	15
PPP3	238	20	8
PPP4	225	10	4
PPP5	220	8	3

3.3. Particle characterization

All samples listed in Table 2 resulted in the formation of spherical multilayered nanostructures. As an example, only characterization results for sample PPP3 are presented in this section. The production of PLGA–PCL–PMSQ tri-layered sub-micron particles was confirmed by the FTIR and NMR spectra presented in Figs. 3 and 4, respectively. FTIR measurements were taken over the range 350–4000 cm^{-1}. The presence of three polymeric components is expected to yield some overlapping peaks, however we can elicit the presence of the components. The spectra exhibited a strong band around 3440 cm^{-1} that can be attributed to CH, CH_2, CH_3 from the methylene units fromPCL, PLGA and the OH stretching from the PMSQ units. Within the peak range of 3000–3500 cm^{-1} the carboxylic acid was identified as PLGA. A strong band at about 1687 cm^{-1} corresponds to the stretching vibration of the C—O bond arising from PLGA and PCL units. The peaks at 2890 and 2980 cm^{-1} can be correlated to the —CH stretch of the methylene groups from the PCL [29]. The bands at 1095 cm^{-1} can be assigned to the C—O—C stretching, with the bands at 1130 cm^{-1}(weak) and 1452 cm^{-1} corresponds to the C—O bond and themethyl group C—H bond (methyl group CH stretching) of PLGA, respectively [13]. Due to the presence of the Si—O—Si backbone from the PMSQ there is considerable overlap with peaks in the 1000–1250 cm^{-1} region and thus it is difficult to assign peaks individually arising from the three different polymer components in this region. The spectra also showed peaks at 800–1300 cm^{-1}, assigned to the typical Si—O bond present in the PMSQ network [30]. In addition, weak absorption bands at around 1275 cm^{-1} for methyl groups (CH_3), further confirmed the presence of PMSQ in the structure [30].

The production of PLGA–PCL–PMSQ tri-layered sub-micron particles was further confirmed by the ^{13}C NMR spectra presented in Fig. 4. The peak observed at 157 ppm can be assigned to the carbonyl group arising from the ester groups present in both PLGA and PCL. A strong high intensity peak centered at 18.8 ppm corresponds to the methyl groups attached to the Si in the PMSQ. Peaks in the regions of 48.5–52.0 ppm are due to CH_2 groups, where CH_2–C are around 48 ppm, since they are less deshielded, and CH_2–O being at the higher range due to oxygen being more

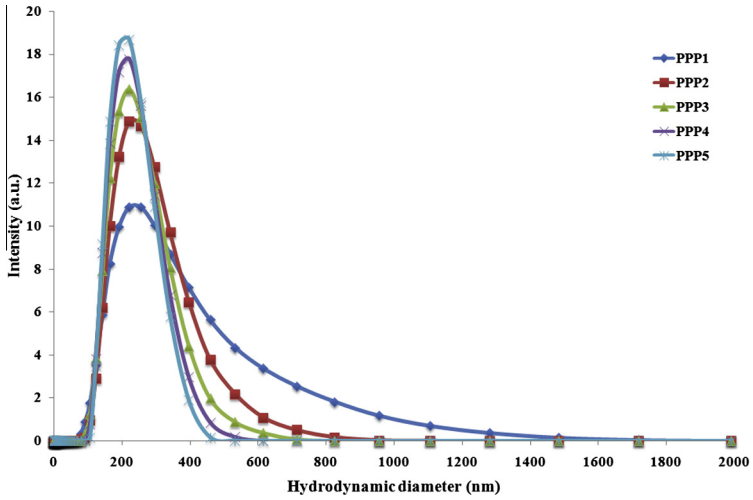

Fig. 2. Dynamic light scattering (DLS) measurements of the size distribution of particles prepared by the EHD process.

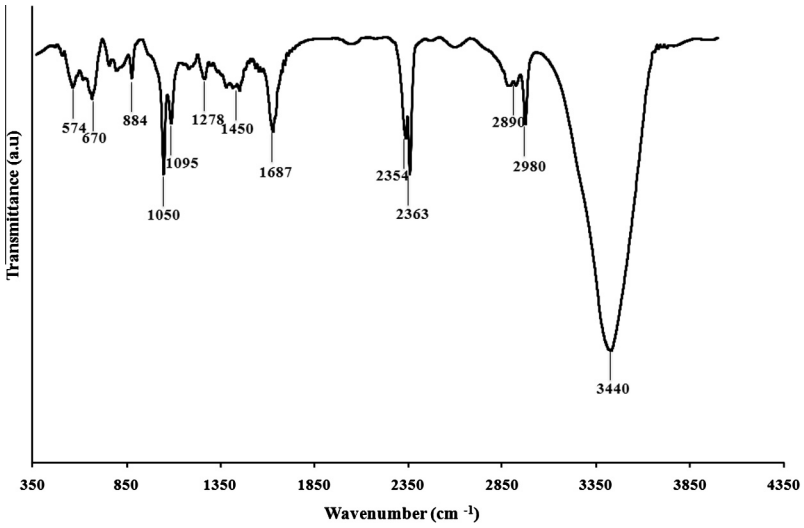

Fig. 3. FTIR spectra of PLGA–PCL–PMSQ particles (sample PPP3).

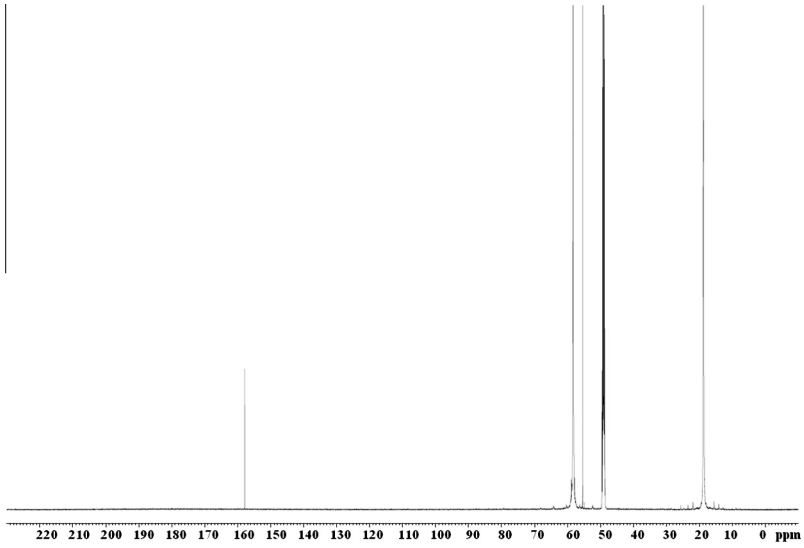

Fig. 4. ^{13}C NMR spectra of PLGA–PCL–PMSQ particles (sample PPP3). *X*-axis is the chemical shift (ppm).

electronegative and more deshielded. This clearly shows the presence of PCL. Within the range of 54.9–65 ppm most CH groups are found which arise from the different polymers present in the particles. The high intensity peak suggests a large number of CH groups from the repeating groups whilst the single peak centered at 55pm is most likely to be from the lactide units of the PLGA. These further confirm the presence of PLGA in the multilayered structure.

The confocal fluorescence micrographs depicted on Fig. 5 are representative images of tri-layer sub-micron particles, each layer labeled accordingly. The confocal microscope was applied to analyze the three layers within the particles. The images clearly indicate that layers exhibited the blue, green and red emission fluorescent signal confirming that the processing technique can successfully produce multilayered sub-micron particles. It is however not possible to visualize and resolve the particles as it is beyond the power of the microscope (based on the current sample preparation) and also the sample being prone to photo bleaching as a result of oxidation. Hence other techniques of FIB–SEM and TEM were applied to study the morphology and internal structure of the produced sub-micron particles in detail.

Fig. 6a shows that, at low magnification, the particles had smooth, spherical and nearly mono-dispersed, non-agglomerated structures. From Fig. 6b, it is clear that the particles possess a tri-layered structure, each layer labeled accordingly. Also, the outer layer (PLGA) showed to be sensitive to beam damage since the layer was gradually disappearing following exposure to the beam (Fig. 6b). This effect was not seen in TEM since the Gallium source in FIB–SEM are heavier ions compared with electrons used in TEM and hence will have a greater impact on the layers leading to beam damage. Previous studies have commonly applied TEM to visualize layered structures. In this study, a typical TEM micrograph of the resultant PLGA–PCL–PMSQ tri-layer sub-micron particle is shown in Fig. 6c and d. The three distinct layers were clearly observed (Fig. 6c and d) with a strong contrast difference between the PLGA (outer), PCL (middle) and PMSQ (inner).

Overall, from both the FIB–SEM and TEM micrographs (Fig. 6a–d) it is apparent that the inner layers are much thicker

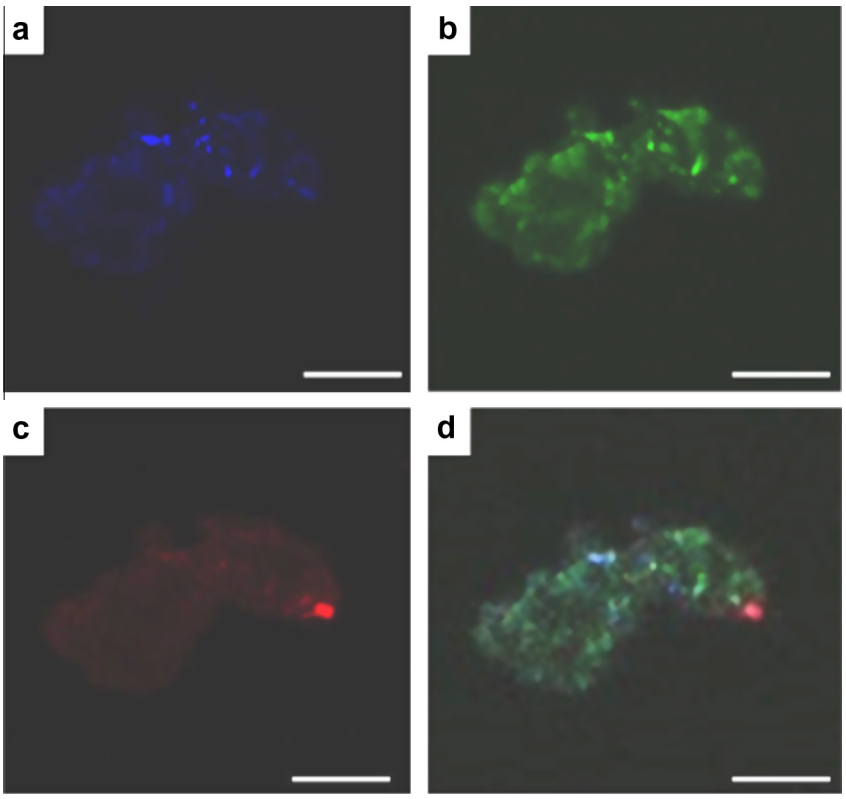

Fig. 5. Confocal images of a collection of labeled PLGA–PCL–PMSQ (PPP3) particles on a glass cover slip. (a) Calcein blue-labeled PLGA (outer layer), (b) methyl green-labeled PCL (middle layer), (c) Evan's blue-labeled PMSQ and (d) overlap of three channels of blue, green and red representing layers of PLGA, PCL and PMSQ, respectively. Scale bar = 25 μm (For interpretation of the references to color in this figure legend, the reader is referred to the web version of this article.).

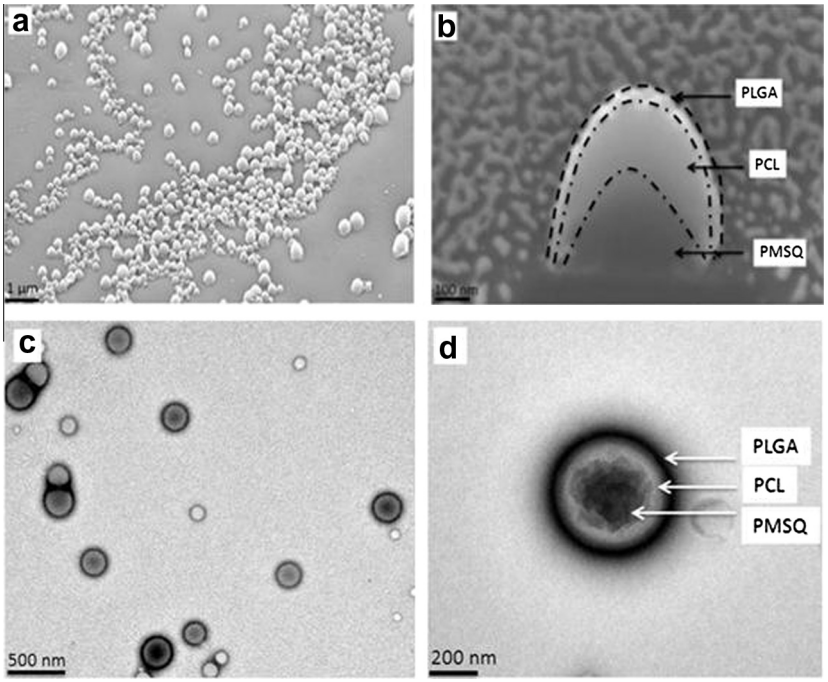

Fig. 6. (a–b) Dual beam FIB–SEM showing the external and internal structure of PLGA–PCL–PMSQ (sample PPP3) particles (a) at low magnification, prior to FIB sectioning and (b) following FIB sectioning on the largest particle in the sample. Dotted lines indicate the different layer boundaries. (c–d) Bright field TEM micrograph of PLGA–PCL–PMSQ (PPP3) particles prepared by EHD processing (a) at low magnification and (c) high magnification, showing the three-layered structure of the particles.

than the outer ones. In addition the graph presented in Fig. 7, which is a representation of particle thickness as a function of radius of individual particles, demonstrates that the outer layer (labeled a on Fig. 7) is smaller in size compared to the middle layer (labeled b in Fig. 7). The overall ratio (gradient of linear regression line in Fig. 7) of the outer layer (0.15) is smaller than middle layer

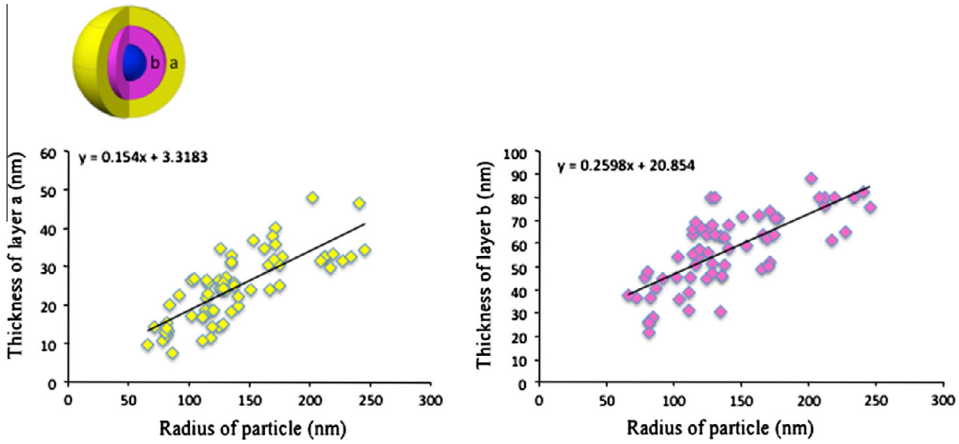

Fig. 7. Two graphs presenting the relationship between the radius of each particle and the corresponding layer thickness (layer *a* or *b*), according to the scheme of the tri-layered nanoparticle (inset), where *a* is the outer layer and *b* is the middle layer. Gradient of line presented on each graph. $n = 70$, where n is the number of particles.

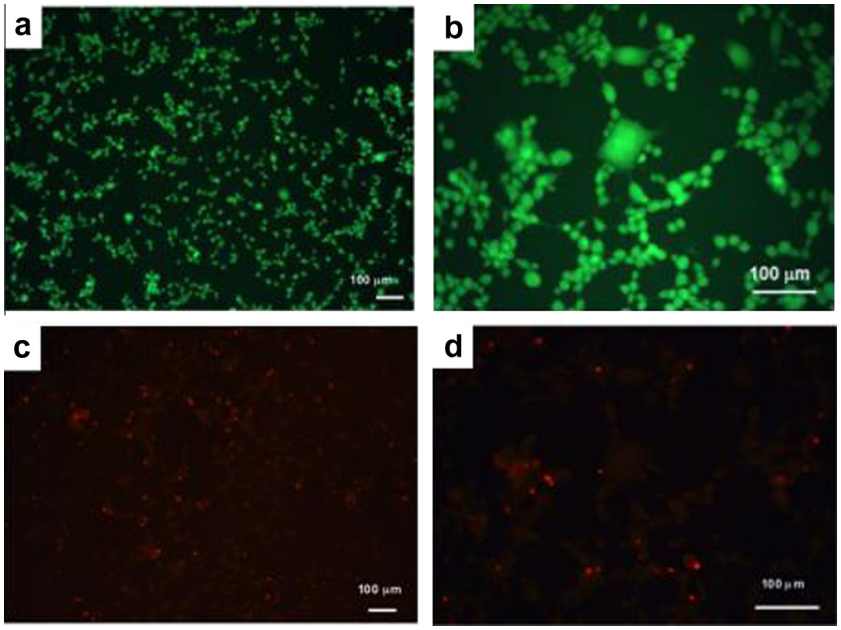

Fig. 8. HOB cells were cultured in the presence of tri-layered particles for 24 h. Cell viability was determined using the (a–d) Live/Dead assay. Samples were visualized using a fluorescence microscope with live (a and b) and dead (c and d) cells staining green (calcein AM) or red (EthD-1) respectively.

(0.26). The difference in thickness between the particles may be attributed to the fact that the inner droplets break up more effectively than the outer ones under appropriate applied voltage and also due the relative volume flow rates of the processing liquid. In addition, according to the graph in Fig. 7, the uniformity between the particles i.e. the outer or inner layer to the overall radius is always a constant ratio. Hence, the current synthesis route enables good control over consistency between layer formation. This is advantageous for future applications of these particles.

3.4. HOB cell's response to tri-layered particles

Cell studies were carried out to establish whether the combination of the three polymers and the corresponding synthesis route results in any possible toxicity. For this purpose, human osteoblast (HOB) cells were used. The live/dead test was also used (Fig. 8a–d). This assay is a commonly used two-color fluorescence-based method for determining viability of adherent or non-adherent cells. The assay measures intracellular esterase activity and

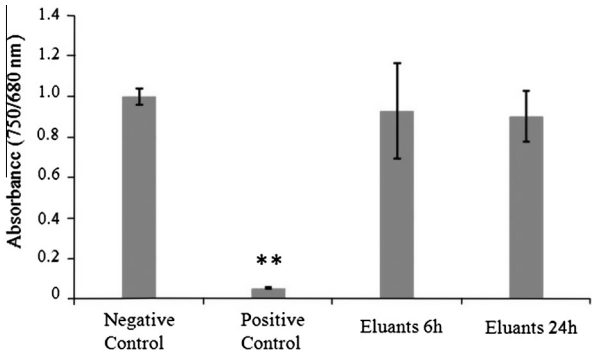

Fig. 9. Cell metabolic activity data measured using an MTT assay after HOB cells were treated with tri-layered particles (100 µl of elution fluid) after 24 h. The eluants were obtained by placing the tri-layered particles in DMEM complete media for 6 and 24 h. The average values obtained for each eluant material were normalized with respect to that of the negative control (cells immersed in media only). Values represent the mean ± SD of experiments each performed in sextuplicate ($^{*}p < 0.01$ relative to negative control, without particles).

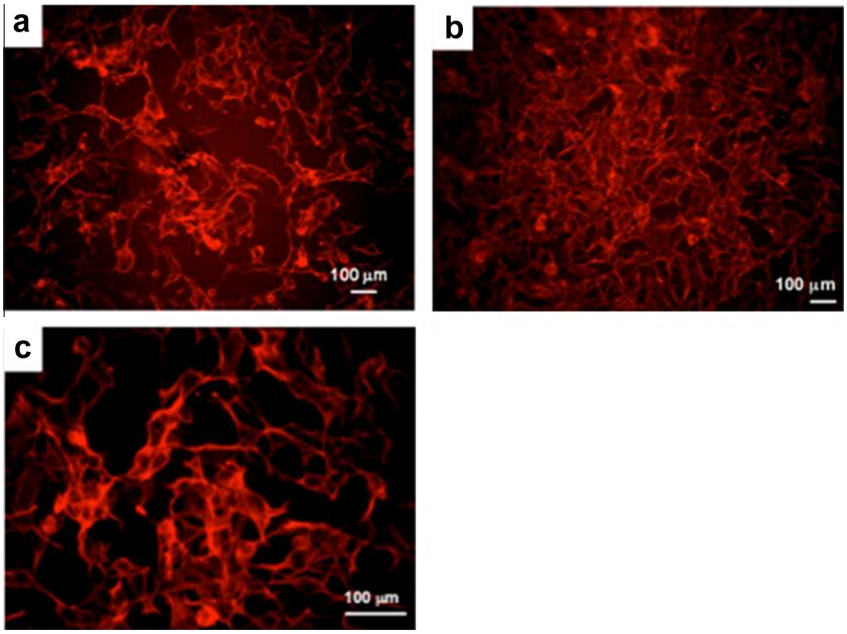

Fig. 10. Fluorescence microscope images of (a and b) HOB cells exposed to tri-layered particles for 24 h. (c) HOBs in the absence of particles. Actin cytoskeleton was stained with Phalloidin-TRITC (red) (For interpretation of the references to color in this figure legend, the reader is referred to the web version of this article.).

staining nucleic acids in chromatin as a mean of plasma membrane integrity. Viable cells indicated via green fluorescence showed that viable cells existed in the presence of the tri-layered sub-micron particles, which confirmed cells had esterase activity with an intact cell membrane. The dead cells are labeled with Ethidium homodimer-1 (EthD-1), which is excluded by the intact plasma membrane of live cells. Fig. 8a and c shows that there were live cells with very few dead cells present, thus indicating that the particles were not having an adverse effect upon the viability of the cells. As the particles on their own also exhibited fluorescence, this masked some of the cells that were taking up the green dye but the image at the higher magnification (Fig. 8b) clearly indicated that live cells were present and very few dead cells were observed. To further assess any possible toxicity of the tri-layered sub-micron particles, the cell metabolic activity of the eluants obtained after 6 and 24 h were subjected to 24 h incubation (Fig. 9) as were the negative and positive controls. The one way ANOVA test showed that at 24 h incubation, cell metabolic activity was significantly higher ($p < 0.01$) compared to the positive control but there were no significant differences with the negative controls. A Kruskal Wallis test showed that the differences in the median values among the treatment groups were not great enough to exclude the possibility that the difference is due to random sampling variability; and there was no statistically significant difference ($P = 0.67$) between the eluants obtained after 6 and 24 h. This confirmed that the sub-micron particles did not leach any toxic components (Fig. 9).

Furthermore, HOB cells were cultured in the presence of the tri-layered sub-micron particles for 24 h and the Actin cytoskeleton was stained with Phalloidin-TRITC and visualized by fluorescence microscopy. Actin is a major component of the cytoplasm, which is usually the most abundant protein in the cell. The images in Fig. 10a and b showed that actin is well organized in the presence of the tri-layered particles and comparable to those on the control, thermanox (Fig. 10c) suggesting that the particles did not inhibit cellular activity. Overall, the cell data presented show that the particles were non-toxic, hence confirming that all solvents had fully evaporated, diffused out, from the particles.

Considerable effort has been devoted to the preparation of multilayered sub-micron particles of various compositions with a controlled size distribution. An important advantage of such sub-micron particles is the encapsulation of functional materials into the structure to provide a desired characteristic/activity. It is believed that the formation of tri-layer sub-micron particles by EHD processing, as presented in this study, is novel and, also, potentially beneficial for drug delivery applications. The different layers provide means of encapsulating different drugs and/or different concentrations in order to tailor the release profile *in vivo*. Similarly, using layers of different matrix materials, would allow independent surface modification, independent control of extremely diverse functionalities, including release rate, environmental responsiveness or antibacterial properties of the sub-micron particles. The ability of the technique to prepare particles at the nanoscale is also an advantage.

4. Conclusions

The capability of the electrohydrodynamic process, in combination with a triple-needle device, was demonstrated for the preparation of nearly mono-dispersed, spherical and tri-layered structures, containing PMSQ, PCL and PLGA in a single step process. Optimized particles had an average size ranging from 320 nm (±80 nm) to 220 (±8 nm), with a change in the processing parameters. A range of characterization techniques including confocal, SEM–FIB and TEM showed the presence of the layered structure. Particles were shown to be non-cytotoxic, indicating their potential suitability for medical applications. It is important to note that the ability to produce such layered structures, using biocompatible polymers, contributes significantly to the pharmaceutical industry. The progression from this study would ultimately lead to great potential in multiple loading of therapeutic agents.

Acknowledgements

The Engineering and Physical Sciences Research Council are thanked for funding this project via grant EP/J01334X/1. Dr David Gathercole and Dr Lina Meghani are thanked for their kind assistance with the confocal microscope and NMR, respectively.

References

[1] Y.C. Wang, S. Gao, W.H. Ye, H.S. Yoon, Y.Y. Yang, Nature Materials 5 (2006) 205–219.
[2] T. Basinska, S. Slomkowski, Bioactive Compatible Polymers 8 (1993) 205–219.
[3] F. Caruso, R.A. Caruso, M. Helmuth, Science 282 (1998) 1111–1114.
[4] S.R. Carter, S. Rimmer, Advanced Functional Materials 14 (2004) 553–561.
[5] Y.W. Zhang, Polymer 48 (2000) 5639–5645.
[6] S. Mitragotri, J. Lahann, Nature Materials 8 (2009) 15–23.
[7] L. Ding, Journal of Controlled Release 102 (2) (2005) 395–413.
[8] R. Pareta, M.J. Edirisinghe, Journal of Royal Society Interface 3 (9) (2006) 573–582.
[9] M.D. Paine, M.S. Alexander, J.P.W. Stark, Journal of Colloid and Interface Science 305 (1) (2007) 111–123.
[10] I.G. Loscertales, A. Barrero, I. Guerrero, R. Cortijo, M. Marquez, A.M. Ganan-Calvo, Science 295 (5560) (2002) 1695–1698.
[11] E.A. Botchwey, S.R. Poack, E.M. Levine, E.D. Johnston, C.T. Laurencin, Journal of Biomedical Material Research Part A 69A (2) (2004) 205–215.
[12] J. Panyam, V. Labhasetwar, Biodegradable nanoparticles for drug and gene delivery to cells and tissue, Journal of Advanced Drug Delivery Rev 55 (3) (2003) 329–347.
[13] H.K. Makadia, S.J. Siegel, Polymers 3 (3) (2011) 1377–1397.
[14] D. Quintanar-Guerrero, E. Allemann, H. Fessi, E. Doelker, Drug Development and Industrial Pharmacy 24 (12) (1998) 1113–1128.
[15] H. Xiang, L. Zhang, Z. Wang, X. Yu, Y. Long, X. Zhang, N. Zhao, J. Xu, Journal of Colloid and Interface Science 359 (1) (2011) 296–303.
[16] U. Farook, E. Stride, M.J. Edirisinghe, R. Moaleji, Medical & Biological Engineering & Computing 45 (8) (2007) 781–789.
[17] J. Xie, W.J. Ng, L.Y. Lee, C.H. Wang, Journal of Colloid and Interface Science 317 (2) (2008) 469–476.
[18] Z. Ahmad, H.B. Zhang, U. Farook, M. Edirisinghe, E. Stride, P. Colombo, Royal Society Interface 5 (27) (2008) 1255–1261.
[19] J.M. López-Herrera, A. Barrero, A. Lopez, I.G. Loscertales, M. Marquez, Scaling laws. Aerosol Science 34 (5) (2003) 535–552.
[20] G. Taylor, Proceedings of the Royal Society of London. Series A. Mathematical and Physical Sciences 280 (1382) (1964) 383–397.
[21] S.N. Jayasinghe, M.J. Edirisinghe, Nanoscience and Nanotechnology 5 (6) (2005) 923–926.
[22] R.P.A. Hartman, J.P. Borra, D.J. Brunner, J.C.M. Marijnissen, B. Scarlett, Electrostatics 47 (3) (1999) 143–170.
[23] L. Di Silvio, N. Gurav, J.R.W. Masters (Eds.), Kluwer Academic Publishers, 2001, pp. 221–241.
[24] B.K. Ku, S.S. Kim, Aerosol Science 33 (10) (2002) 1362–1378.
[25] M. Cloupeau, B. Prunet-Foch, Electrostatics 22 (2) (1989) 135–159.
[26] N. Bock, M. Woodruff, D.W. Hutmacher, T.R. Dargaville, Polymers 3 (1) (2011) 131–149.
[27] P. Gupta, C. Elkins, T.E. Long, G.L. Wilkes, Polymer 46 (13) (2005) 4799–4810.
[28] G. Raos, G. Allegra, Chemical Physics 104 (4) (1996) 1626–1645.
[29] T. Elzein, M.N. Eddine, C. Delaite, S. Bistac, P. Dumas, Journal of Colloid and Interface Science 273 (2) (2004) 381–387.
[30] M.W. Chang, E. Stride, M. Edirisinghe, Society Interface 7 (Suppl 4) (2010) 451–460.